Journal of Rehabilitation in Civil Engineering 13-4 (2025) 47-66

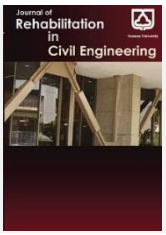

Journal of Rehabilitation in Civil Engineering

Journal homepage: https://civiljournal.semnan.ac.ir/

Incremental Dynamic Analysis of Mid-Rise Buildings with Buckling Restrained Brace Frame System under Pulse-Like Near-Fault Ground Motions

Yaghub Minaei [1]; Mohammadreza Mashayekhi [2*]; Mohammad Sarcheshmehpour [3]

1. Department of Civil Engineering, Technical and Vocational University (TVU), Tehran, Iran
2. Department of Civil Engineering, K. N. Toosi University of Technology, Tehran, Iran
3. Department of Civil and Environmental Engineering, Shiraz University, Shiraz, Iran
* Corresponding author: *m.mashayekhi@kntu.ac.ir*

ARTICLE INFO

Article history:
Receive: 10 May 2024
Revise: 24 December 2024
Accept: 14 January 2025

Keywords:
Buckling restrained braced frame;
Near-Field ground motion;
Nonlinear dynamic analysis;
Incremental dynamic analysis.

ABSTRACT

Buckling Restrained Braced Frames (BRBFs) are frequently utilized as seismic force-resisting systems due to their considerable ductility and energy dissipation capacity. While BRBFs have shown reliable seismic performance in extensive experimental and numerical studies under far-field ground motions, research on their performance under near-fault ground motions is limited. near-fault ground motions, characterized by short-duration pulses with high amplitudes, impose greater seismic demands on structures. This study conducts Incremental Dynamic Analysis (IDA) on two 8- and 12-story BRBF structures under far-fault and near-fault ground motions. Comparison involves confidence intervals of average IDA curves rather than direct curve comparisons due to record selection uncertainty. At 99% confidence, no significant differences are observed. At 95% confidence, a minor difference is noted, while at 90%, substantial differences emerge, with confidence intervals indicating about a 25% difference for the 8-story and 75% for the 12-story structure. Residual drift comparisons show no significant difference at 99% confidence, a slight difference for the 12-story structure at 95%, and significant differences for both structures at 90% confidence. This suggests the importance of considering near-fault ground motions in assessing BRBF seismic performance, particularly for taller structures.

E-ISSN: 2345-4423

How to cite this article:
Minaei, Y., Mashayekhi, M. and Sarcheshmehpour, M. (2025). Incremental Dynamic Analysis of Mid-Rise Buildings with Buckling Restrained Brace Frame System under Pulse-Like Near-Fault Ground Motions. Journal of Rehabilitation in Civil Engineering, 13(4), 47-66. https://doi.org/10.22075/jrce.2025.33814.2044

1. Introduction

A Buckling Restrained Brace (BRB) comprises a steel core and a casing designed solely to prevent the steel core from buckling. To avoid the transfer of axial forces to the casing, a debonding material or an empty gap is placed between the core and the casing. The main idea behind the Bucking Restrained Braced Frame (BRBF) as a relatively new seismic lateral resisting system was formed based on preventing the buckling of braces in the conventional CBF system. In this regard, steel braces have undergone a number of improvements, including the usage of an enclosed steel brace and combinations of a steel tube, filler, and unbounding substance to prevent buckling. The BRBF system has emerged as a popular alternative to the conventional CBF system for the seismic-resistant building design. The BRBF system was first introduced in the 80s in Japan [1–3], but its use in America dates back to after the 1994 Northridge earthquake [4].

The traditional CBF system exhibits unsymmetrical hysteretic behavior with significant strength deterioration because the tension and compression behavior of the braces is different. But, with the BRBF system, braces can yield in both tension and compression. Black et al. [5] demonstrated that the BRBF system offers significant and repeatable energy dissipation capabilities in addition to the stiffness required to satisfy the permitted drift limits in buildings as compared to the CBF system. The BRBF system exhibits stable and predictable hysteretic behavior and provides significant energy dissipation capacity and ductility. This feature of the BRBF system has attracted a lot of interest across the world. Xie [6] states that the BRBF technology is used in the construction of about 60% of steel high rise buildings in Japan. In addition to using the BRBF system for new buildings, this system can be also used in retrofitting existing structures. For example, Carden [7] used the BRB system to upgrade steel bridges. Castaldo [8] used the BRBF system as a means of rehabilitating or upgrading numerous existing reinforced concrete framed structures.

Early studies on the BRBF system focused on the BRB element alone, independent of the frame [9–11]. The ductility of the element was investigated, and the results indicated the high ductility of the element. Mirtaheri et al. [12] optimized the length of BRB steel core to increase the dissipation energy capacity of the member. Chen et al. [13] investigated the effect of the unbounding materials on the performance of BRBs. In other researches, the hysteretic behavior and ductility of BRBF system were investigated in large-scale tests in which the BRB elements are parts of full frames [14–18].

Another group of research investigated the performance of the BRBF system computationally. Sabelli et al.[19] did numerical research on BRBFs which demonstrated that the residual story drifts are approximately 40 to 60 percent of the highest drift values. Tremblay and Poncet [20] conducted research to compare the seismic behavior of conventional CBFs and BRBFs. Kiggins and Yuang [21] investigated the use of the BRBF system in a dual system to minimize permanent residual deformation. Fahnestock et al. [22] describes numerical simulation of the BRBF system to analyze the response under strong ground motions. Naghavi et al. [23] compared the performance of the BRBF system with traditional CBF structures through numerical investigation. Asgarkhani et al. [24] proposed four approximate methods for estimating residual drift demands in BRBFs. Asgarian and Shokrgozar [25] evaluated overstrength, ductility, and response modification of BRBF structures. Ariyaratana and Fahnestock [26] employed nonlinear dynamic analysis to evaluate the performance of BRBF and BRBF-SMRF systems. Li et al. [27] conducted a series of hybrid and cyclic loading tests on a three-story single-bay full-scale BRBF.

Even though BRBFs have been the subject of numerous studies examining their seismic behavior, very few studies have been conducted on the effect of the type of strong ground motions on the

response of BRBFs. The effectiveness of BRBF structures needs to be examined in relation to the influence of various types of strong ground motions. Near-field strong ground motions are one of the various types of strong ground motions that have distinctive properties. Near field ground motions are described as ground motions that occur when the earthquake's epicenter is close to the desired site. To distinguish between far-field and near-field ground motions, the base distance from the fault rupture is 20 kilometers. Examples of near-field ground motions have been seen in Northridge (1994), Kobe (1995), Kokaeli-Turkey (1999), and Chi-Chi Taiwan (1999). When the fault rupture propagates towards the site, typically at a velocity close to the shear wave velocity, near-fault ground motions can be identified by large, long-period velocity pulses in the fault-normal direction. In contrast to far-fault earthquakes, a significant amount of seismic energy is released in a short time at the "forward-directivity" site, leading to much higher demands for engineering structures [28,29]. Another common near-fault ground motion characteristic known as "fling step" is characterized by a unidirectional large-amplitude velocity pulse with a permanent offset of the ground. It occurs parallel to strike or dip directions [30]. Fling step ground motions exhibit one-sided pulses that cause permanent ground displacement, whereas forward directivity ground motions feature two-sided pulses and do not result in permanent displacement. The displacement history of the ground motions of filing steps exhibits a monotonic step. Structures may experience residual displacement as a result of these monotonous steps.

One of the most defining features of near-fault ground motions is the presence of a pulse in their velocity time history. Numerous studies have been conducted to identify these pulses, classifying such ground motions as pulse-like. Among these studies, Baker's work [31] is particularly noteworthy. Wavelet analysis was used to extract the largest pulse from the velocity time history, and the size of the extracted pulse, relative to the original ground motion, was quantified. This comparison provided a criterion for determining whether a ground motion is classified as pulse-like. Hoseini Vaez and Minaei [32] applied Particle Swarm Optimization (PSO) to extract velocity pulses across a broad range of pulse-like ground motions. Minaei et al. [33] employed a mathematical model combined with the Imperialist Competitive Algorithm (ICA) to extract the dominant pulse from pulse-like records. Vaez et al. [34] proposed a new mathematical method consisting of two components: harmonic and polynomial expressions, designed to simulate the dominant velocity pulse of near-fault ground motions.

The impact of near fault ground motions on the performance and seismic response of BRBFs structures has not been the subject of many studies. Vafaei and Eskandari [35] investigated the seismic performance of steel BRBFs with mega configuration under near source excitation. Du et al. [36] presents the seismic performance quantification of BRBs and reinforced concrete frames as a dual system subjected to near-fault ground motions with forward-directivity and fling step effects. According to Fang et al. [37], near-fault pulse type motions increased the deformation demand in the BRBs but did not result in a larger floor acceleration. Ahmad and Phillips [4] investigated the response of BRBF buildings under four ground motion sets, which are far fault, near fault with pulse, near fault with no pulse, and subduction zone long duration earthquakes. Shakouri et al. [38] investigated the impact of seismic pounding between adjacent structures isolated with double friction pendulum bearings (DFPB) and triple friction pendulum bearings (TFPB) under near-fault ground motions. Majdi et al. [39] investigated the effect of near-fault earthquake characteristics on the seismic response of structures isolated with Triple friction pendulum isolator. Soltanmohammadi et al [40] investigated the effect of near fault ground motions on the fragility curves of multi-span simply supported concrete girder bridges. Minaei et al. [41] proposed a method for estimating the response of steel moment-resisting frames subjected to pulse-like ground motions.

Although the results of these research studies serve as useful guidelines, they do not consider the impact of near-fault ground motions on the response of BRBF structures at multiple intensity measures (IMs). The impact of near-fault ground motions on the response of BRBF structures has only been examined at one intensity level in all of the aforementioned studies. IDA is the time history dynamic analysis in which the response of structures is obtained at various IMs. This useful analysis method was first introduced by Vamvatsikos and Cornell [42]. IDA entails executing numerous nonlinear dynamic analyses on a structure while gradually intensifying the input ground motion until the structure reaches a predetermined limit state.

In this study, the effect of near-fault ground motions on the seismic demands of mid-rise BRBF structures is investigated. Seismic demand is calculated using IDA method. In this study, two buildings with a total height of 8 and 12 stories and designs that adhere to the Iranian National Building Code are used as case studies. These two structures were chosen because their periods fall within the range of the pulse periods of near-fault ground motions. Seven ground motions from each of two groups of far-fault and near-fault motions are chosen. Under both near-fault and far-fault ground motions, the IDA curves of these two structures are computed and compared. Owing to the inherent uncertainty stemming from record selection, an alternative approach is taken, whereby the confidence intervals of the averaged IDA curves are contrasted across three distinct confidence levels (99%, 95%, and 90%) for both far-fault and near-fault ground motions. Furthermore, the confidence interval for the distribution of average inter-story drift ratios across the floors is presented and juxtaposed between the two record categories, evaluated at confidence levels of 99%, 95%, and 90%.

2. Structural modeling

In this study, the effect of near-fault ground motions on the IDA curve of BRBF structures is investigated through an examination of two buildings: an 8-story and a 12-story structure, each comprising four spans. In both structures, the first floor's height is set at 5 meters, while the rest of the floors have a uniform height of 4.5 meters. The configuration of these two structures is depicted in Fig. **1** and Fig. **2**. Both of these structures are designed in accordance with the fourth edition of Iranian seismic code (Iranian Code No. 2800 [43], considering a location in Tehran with very high relative seismicity, soil conditions of type III, and an importance factor of I=1. According to Iranian Code No. 2800, the design earthquake's Peak Ground Acceleration (PGA), representing an earthquake with a 10% probability of occurrence in 50 years, is specified as 0.35g. The response modification factor for the BRBF structural system is set at 7. The floor dead load is 640 kg/m², accompanied by a live load of 200 kg/m², along with a snow load of 150 kg/m².

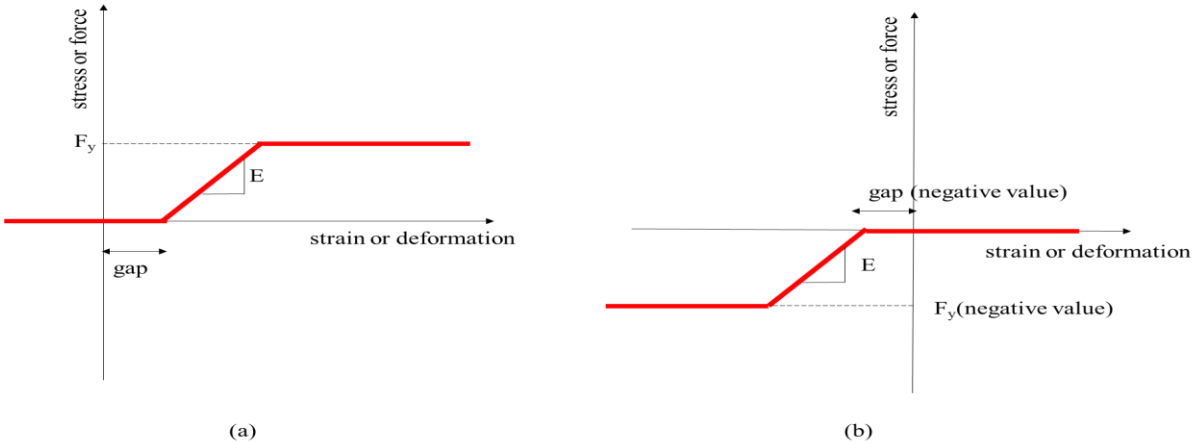

Fig**. 3.** Behavioral model of Elastic-Perfectly Plastic Gap Material (a) tension gap, (b) compression gap.

and

Table **2** illustrate the beam and column sections, and BRBs area in the 8-Story and 12-Story structures, respectively. In this study, the OpenSees software [44] is employed to simulate structures. Floors are modeled using rigid diaphragms, and the connection of the columns to the foundation is assumed to be fixed. The connections of beams to columns are assumed to be simple. The Corotruss element has been utilized for modeling BRB (Buckling Restrained Brace) elements within the OpenSees software. An Elastic-Perfectly Plastic Gap Material is used to model the beam and column. Fig. **3** illustrates the behavioral model of the Elastic-Perfectly Plastic Gap Material. The Fatigue material in OpenSees was used to model the bracing elements. The steel used in the structure have a compressive strength of 290 MPa, an elastic modulus of 199,996 MPa, and a strain hardening value of 0.027.

Table **3** showcases the periods of the first to third modes for both 8-story and 12-story structures.

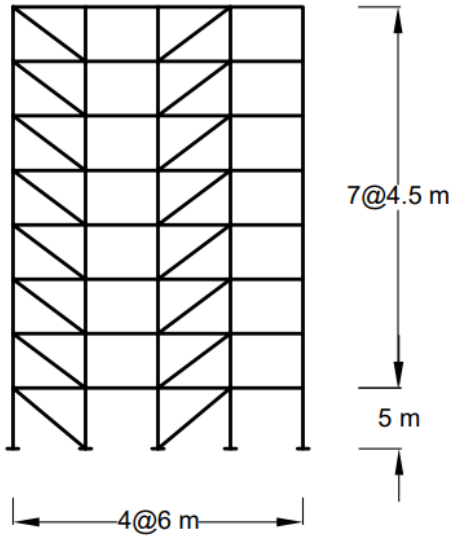

Fig. 1. Height configuration of the 8-story structure.

3. Ground motions selection

To perform IDA analysis for structures, a selection of fourteen records is made, consisting of seven far-fault ground motions and seven near-fault ground motions. All ground motions are of a magnitude of more than 6.5 and belong to soil type III according to Iranian Code No. 2800 (Fourth Edition) [43]. In this study, Kalkan et al.'s [45] recommendations are utilized for selecting near-fault ground motions. Selected far-fault ground motions are all located at distances greater than 10 km from the source. All records are available on the website (http://peer.berkeley.edu/nga). In two-dimensional IDA analysis, the larger horizontal component of the records is employed. Table 1. Beam and column sections, along with BRBs area, in 8-story structure.

Story Number	Brace Area (cm²)	Beam Sections	Columns Sections
8	29	W460x89	W360x110
7	29	W535x124	W360x110
6	45.2	W535x124	W360x216
5	45.2	W535x124	W360x216

4	58.1	W535x124	W360x216
3	58.1	W535x124	W360x347
2	71	W535x124	W360x347
1	71	W535x124	W360x347

Table 2. Beam and column sections, along with BRBs area, in 12-story structure.

Story Number	Brace Area (cm²)	Beam Sections	Column Sections
12	45.2	W460x89	W360x347
11	45.2	W535x124	W360x347
10	45.2	W535x124	W360x347
9	45.2	W535x124	W360x347
8	83.9	W535x124	W360x509
7	83.9	W535x124	W360x509
6	83.9	W535x124	W360x509
5	83.9	W535x124	W360x509
4	96.8	W535x124	W460x463
3	96.8	W535x124	W460x463
2	96.8	W535x124	W460x463
1	96.8	W535x124	W460x463

Table 3. Periods of the first to third modes for the studied structures.

Mode Number	Period (sec)	
	8-story	12-story
1	1.52	2.4
2	0.46	0.7
3	0.23	0.35

and **Error! Reference source not found.** present the characteristics of the far-fault and near-fault ground motion records, including magnitude, average shear wave velocity at upper 30 meters, and distance from the source. In these tables, R_{rup} represents the shortest distance from the recording site to the ruptured area.The acceleration spectra for far-fault and near-fault ground motions are depicted in Fig. **4** and Fig. **5**, respectively. Fig. **6** displays a comparison between the average acceleration spectra of far-fault ground motions and near-fault ground motions. Based on the pulse indicator for classifying ground motions proposed by Kardoutsou et al., [46] all selected near-fault ground motions are classified as pulse-like. As an example, Fig. **7** shows the velocity time history of record number 2 along with its extracted pulse.

4. Results

To construct the IDA curve for the structures, the spectral acceleration at the first mode period considering 5% damping ratio ($S_a(T_1,5\%)$) is selected as the IM, while the engineering demand parameter (EDP) chosen is the inter-story drift ratio. In both two-dimensional IDA analyses with far-fault and near-fault ground motions, the larger horizontal component is employed. **Fig. 8** and **Fig. 9** display the IDA curve for 8 and 12-story structures separately under far-fault and near-fault ground motions. The results exhibit a significant degree of dispersion. Instead of directly comparing their averages, the comparison between IDA curves related to far-fault and near-fault ground motions involves the comparison of their average values' confidence intervals. The rationale behind using confidence intervals, as opposed to point estimates of averages, arises from the presence of inherent uncertainty in the sampling process. A confidence interval represents a range within which the mean of a quantity is expected to fall, based on a specified level of confidence. A direct

comparison of sample means does not account for variability or uncertainty in the data. Two sample means might differ, but this difference could be due to random sampling error. The confidence interval (CI) for estimating the population mean of a quantity can be determined using the following equation:

$$CI = \bar{X} \pm t_{\frac{\alpha}{2}}\left(\frac{S}{\sqrt{n}}\right) \quad (1)$$

Here, $\bar{X}$ represents the mean of a quantity measured from a sample of size n; S denotes the standard deviation of the sample; and $t_{\alpha/2}$ is the t-value from the Student's t-distribution, which corresponds to the chosen significance level (α) for the estimation. For example, if the confidence interval (CI) of interest is 95%, α is set to 0.05.

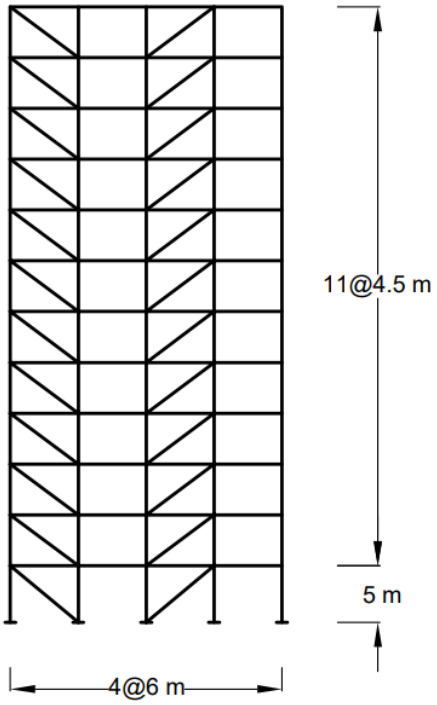

Fig. 2. Height configuration of the 12-story structure.

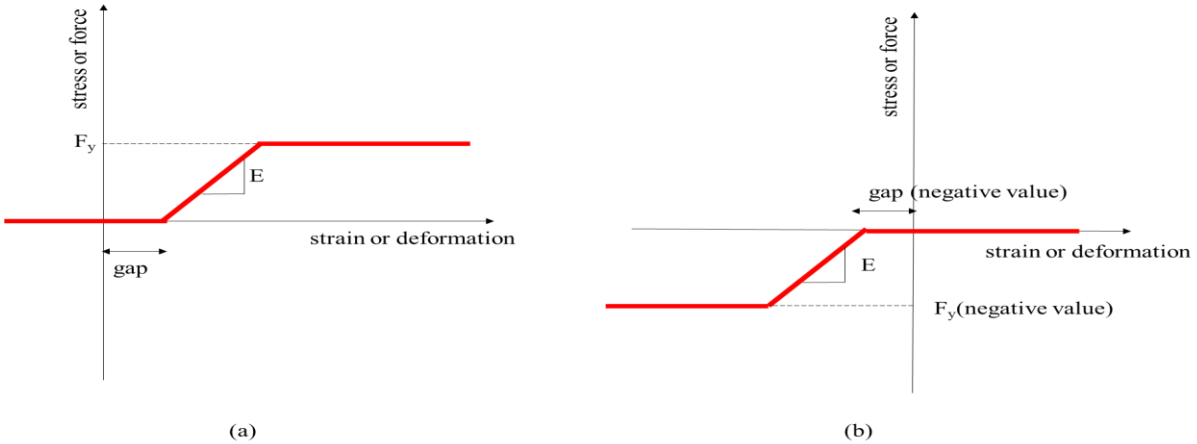

Fig. 3. Behavioral model of Elastic-Perfectly Plastic Gap Material (a) tension gap, (b) compression gap.

Table 1. Beam and column sections, along with BRBs area, in 8-story structure.

Story Number	Brace Area (cm²)	Beam Sections	Columns Sections
8	29	W460x89	W360x110
7	29	W535x124	W360x110
6	45.2	W535x124	W360x216
5	45.2	W535x124	W360x216
4	58.1	W535x124	W360x216
3	58.1	W535x124	W360x347
2	71	W535x124	W360x347
1	71	W535x124	W360x347

Table 2. Beam and column sections, along with BRBs area, in 12-story structure.

Story Number	Brace Area (cm²)	Beam Sections	Column Sections
12	45.2	W460x89	W360x347
11	45.2	W535x124	W360x347
10	45.2	W535x124	W360x347
9	45.2	W535x124	W360x347
8	83.9	W535x124	W360x509
7	83.9	W535x124	W360x509
6	83.9	W535x124	W360x509
5	83.9	W535x124	W360x509
4	96.8	W535x124	W460x463
3	96.8	W535x124	W460x463
2	96.8	W535x124	W460x463
1	96.8	W535x124	W460x463

Table 3. Periods of the first to third modes for the studied structures.

Mode Number	Period (sec)	
	8-story	12-story
1	1.52	2.4
2	0.46	0.7
3	0.23	0.35

In the context of the IDA curve, "sampling" refers to the selection of records. The confidence interval associated with the average establishes a range within which the average is likely to reside, with a given probability denoted as α. This utilization of confidence intervals enhances the robustness of the analysis within the framework of the IDA curve. The application of confidence intervals to compare the IDA curve of far-fault ground motions with that of near-fault ground motions offers a distinct advantage. This lies in its ability to quantify the level of confidence in discerning differences between these two categories.Fig. **10**, Fig. **11**, and Fig. **12** illustrate the contrast in average confidence intervals for IDA curves between far-fault and near-fault ground motions, showcasing confidence levels of 99%, 95%, and 90%. The findings underscore a lack of significant disparity between ground motions in both near-fault and far-fault categories, as indicated by the 99% confidence level results. The confidence intervals of both sets of records intersect, underscoring the absence of a substantial divide. At the 95% confidence level, a slight divergence becomes evident; the confidence intervals no longer overlap, though the observed difference remains minor. Yet, a noteworthy contrast emerges at the 90% confidence level in the responses recorded within these two categories. In addition to the comparison of IDA curves, the study also examines the structural performance at the corresponding intensity level of the Design Based Earthquake (DBE) defined by the Iranian Code No. 2800.

Table 4. Characteristics of far-fault ground motions employed in this study.

Record Number	Event	Year	Station	Mw	Rrup(km)	T_P(sec)	PGA(g)
1	Chuetsu-Oki	2007	Kashiwazaki NPP_ Unit 1: ground surface	6.8	11.00	0.34	0.91
2	El Mayor-Cucapah	2010	Riito	7.2	13.71	0.12	0.39
3	El Mayor-Cucapah	2010	Cerro Prieto Geothermal	7.2	11.00	0.10	0.29
4	El Mayor-Cucapah	2010	Michoacan De Ocampo	7.2	16.00	0.24	0.54
5	Loma Prieta	1989	Gilroy Array #4	6.9	14.34	0.44	0.42
6	Morgan Hill	1984	Gilroy Array #4	6.2	11.54	0.24	0.35
7	Northwest China-03	1997	Jiashi	6.1	17.73	0.20	0.30

Table 5. Characteristics of near-fault ground motions employed in this study.

Record Number	Event	Year	Station	Mw	Rrup(km)	T_P(sec)	PGA(g)
1	Loma Prieta x	1989	LGPC	6.93	3.88	0.70	0.57
2	Kocaeli_ Turkey	1999	Yarimca (YPT)	7.51	4.83	0.52	0.23
3	Chi-Chi_ Taiwan	1999	TCU052	7.62	0.66	1.08	0.36
4	Chi-Chi_ Taiwan	1999	TCU068	7.62	0.32	0.42	0.51
5	Chi-Chi_ Taiwan	1999	TCU074	7.62	13.46	0.70	0.60
6	Chi-Chi_ Taiwan	1999	TCU084	7.62	11.48	0.88	1.00
7	Chi-Chi_ Taiwan	1999	TCU129	7.62	1.83	0.24	1.00

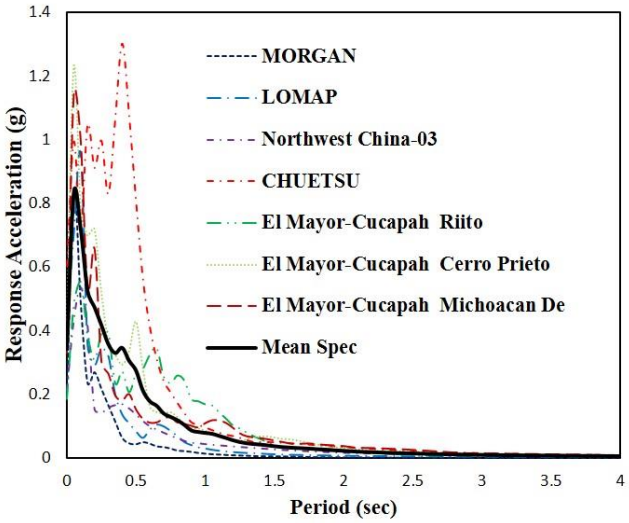

Fig. 4. Acceleration spectrum of far-fault ground motions employed in this study.

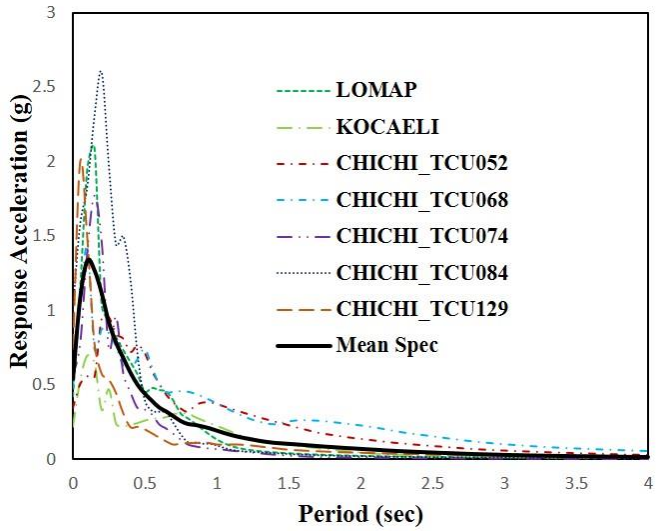

Fig. 5. Acceleration spectrum of near-fault ground motions employed in this study.

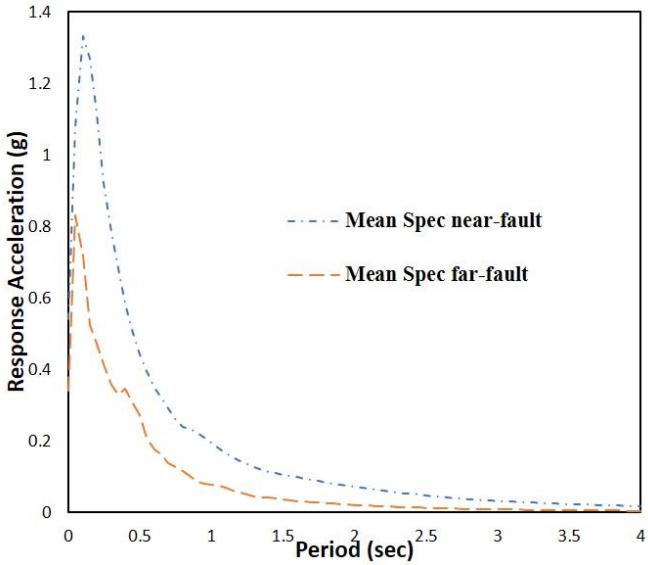

Fig. 6. Comparing the average acceleration spectra of far-fault and near-fault ground motions.

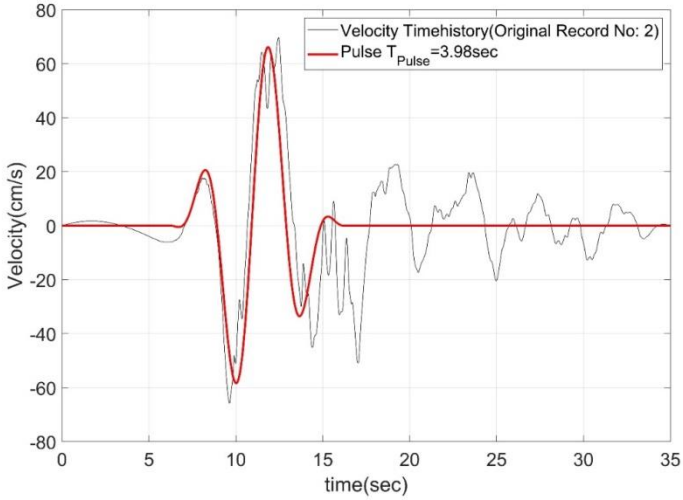

Fig. 7. Velocity time history of a near-fault ground motion employed in the study (Record Number 02).

This evaluation entails a detailed investigation into the distribution of inter-story drift ratios across various floors. Fig. **13** and Fig. **14** depict the inter-story drift ratio distribution across floors for both 8- and 12-story structures, considering both far-fault and near-fault ground motions. The specified threshold for inter-story drift ratio in Iranian Code No. 2800 stands at 2%. According to these figures, observations reveal that within 8- and 12-story configurations, this ratio remains below 2% for all far-fault ground motions. However, for two near-fault ground motions, the maximum inter-story drift ratio of some lower stories in both structures exceeds the allowable limit. Across all four graphs, a notable level of dispersion is evident. To assess the divergence between the performance levels of each designed structure under far-fault and near-fault ground motions, and to determine their compliance with the anticipated limits of the Iranian Code No. 2800 standard, confidence intervals for the inter-story drift ratio are plotted across different floors at confidence levels of 99%, 95%, and 90%. These intervals are then contrasted with the Iranian Code No. Iranian Code No. 2800 limits. Fig. **15**, Fig. **16**, and Fig. **17** present the confidence intervals pertaining to the mean inter-story drift ratios across various floors within both 8 and 12-story structures. These assessments encompass far-fault and near-fault ground motions, scaled to match DBE intensity level. As anticipated, higher confidence levels correspond to larger interval lengths. Notably, the 99% confidence interval is significantly wider than both the 95% and 90% intervals. Therefore, ensuring that these structures uphold an inter-story drift ratio within acceptable limits becomes significantly more demanding at higher confidence levels, particularly under the 99% confidence interval compared to the 95% and 90% intervals. Both considered structures impeccably adhere to regulatory standards across confidence levels of 99%, 95%, and 90%.

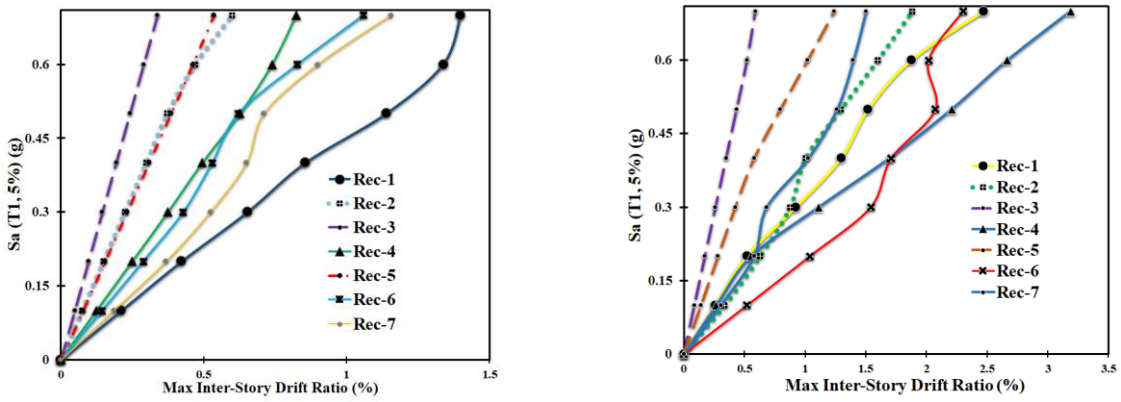

(a) (b)

Fig. 8. IDA curve for the 8-story structure subjected to the selected: (a) far-fault ground motions and (b) near-fault ground motions.

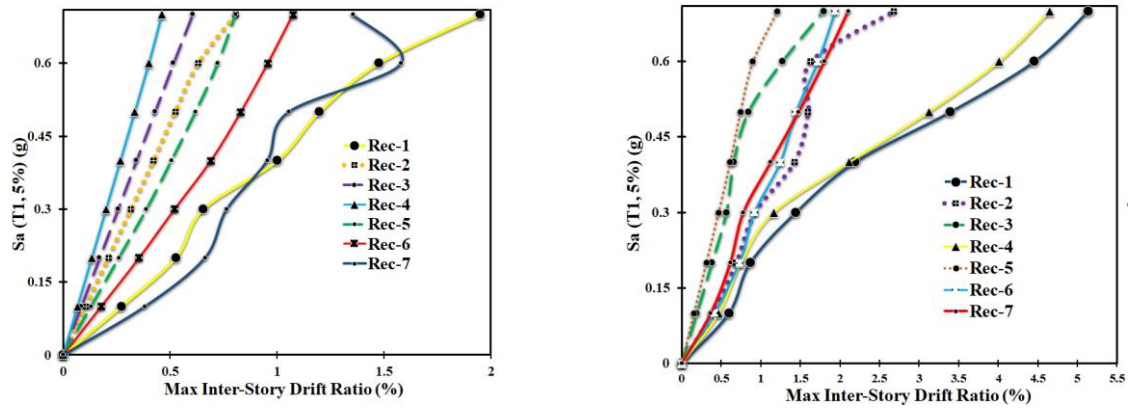

(a) (b)

Fig. 9. IDA curve for the 12-story structure subjected to the selected: (a) far-fault ground motions and (b) near-fault ground motions.

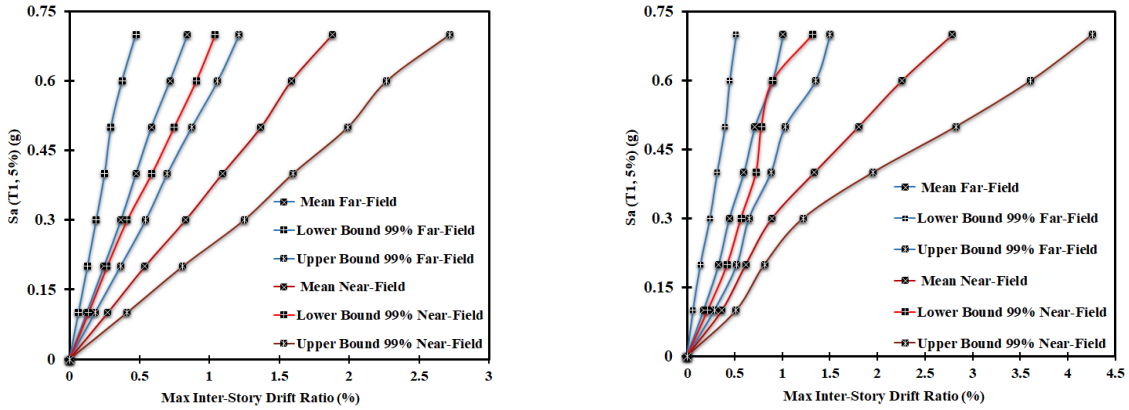

(a) (b)

Fig. 10. Comparing 99% confidence intervals for average IDA curves of far-fault and near-fault ground motions: (a) 8-story structure, and (b) 12-story structure.

Upon analyzing the confidence intervals for inter-story drift ratio of different floors, no notable distinction becomes apparent between the two sets of records at the 99% confidence level. This outcome stems from the overlap of confidence intervals for near-fault and far-fault ground motions. In contrast, at the 95% confidence level, a slight difference is observed in floors 1 to 4 of 8-story structure—where the highest inter-story drift ratios are observed—between the confidence intervals for near-fault and far-fault motions. At the 90% confidence level, no meaningful difference is discernible in both structures within the upper floors.

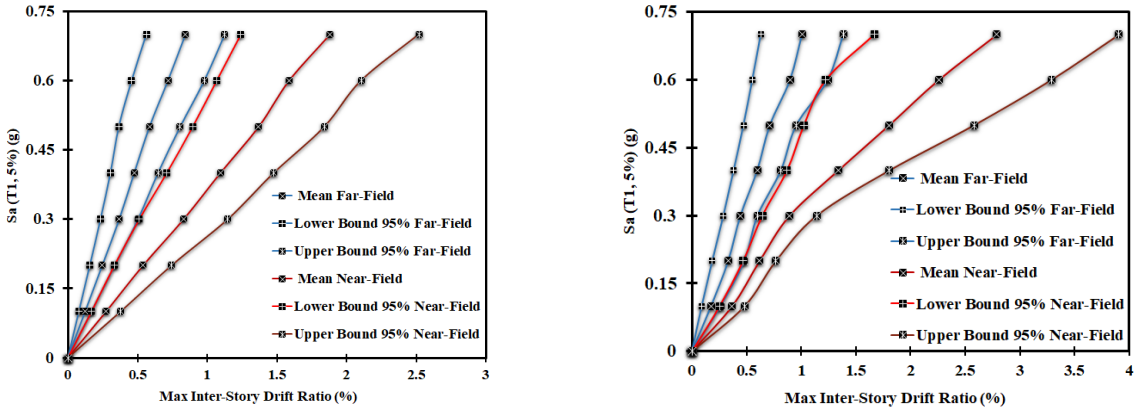

(a) (b)

Fig. 11. Comparing 95% confidence intervals for average IDA curves of far-fault and near-fault ground motions: (a) 8-story structure, and (b) 12-story structure.

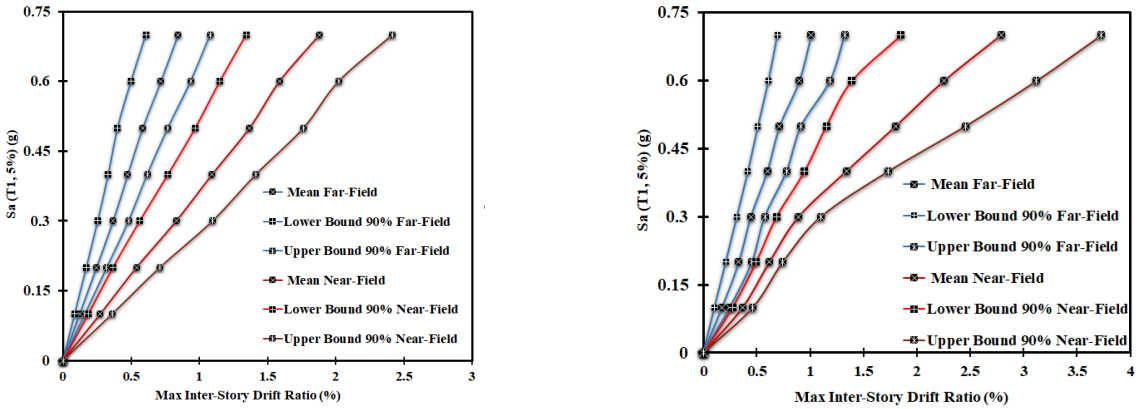

(a) (b)

Fig. 12. Comparing 90% confidence intervals for average IDA curves of far-fault and near-fault ground motions: (a) 8-story structure, and (b) 12-story structure.

Specifically, for floors 1 to 4 of 8-story structure, and also floors 1 to 3 of 12-story structure, which display the most pronounced inter-story drift ratios, the confidence intervals for near-fault and far-fault ground motions do not overlap, indicating a substantial contrast between these categories. An intriguing aspect concerning the contrast between the inter-story drift ratio distribution under far-fault and near-fault ground motions is that beyond the actual values of the drift ratio, the distribution's shape varies. Notably, for near-fault ground motions, the drift on the first and second floors significantly surpasses that of other levels, exhibiting a leaning towards the soft-story mechanism.

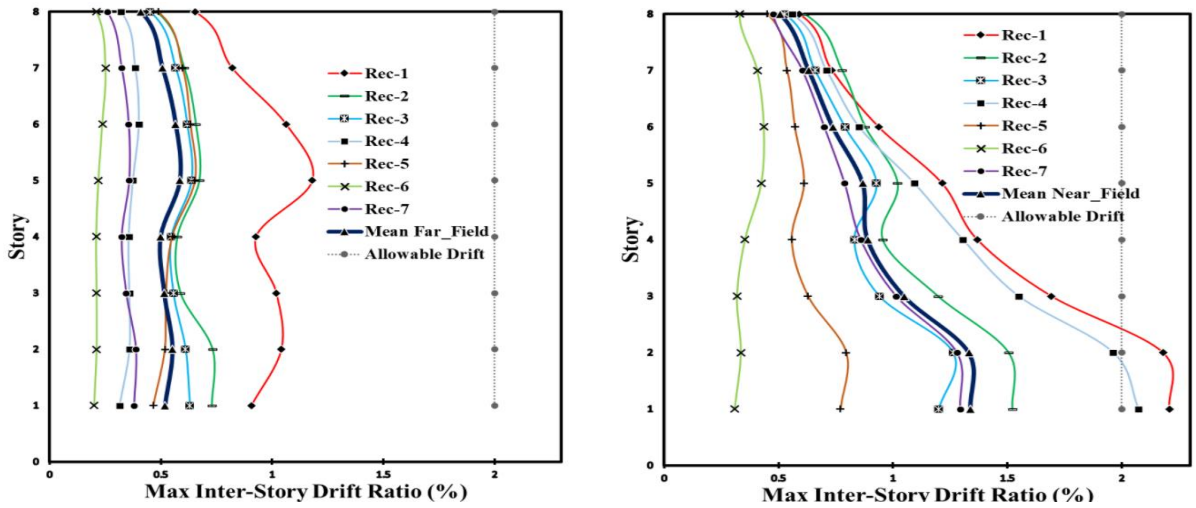

(a) (b)

Fig. 13. Inter-story drift ratio distribution in the 8-story structure under ground motions at DBE intensity level: (a) far-fault and (b) near fault.

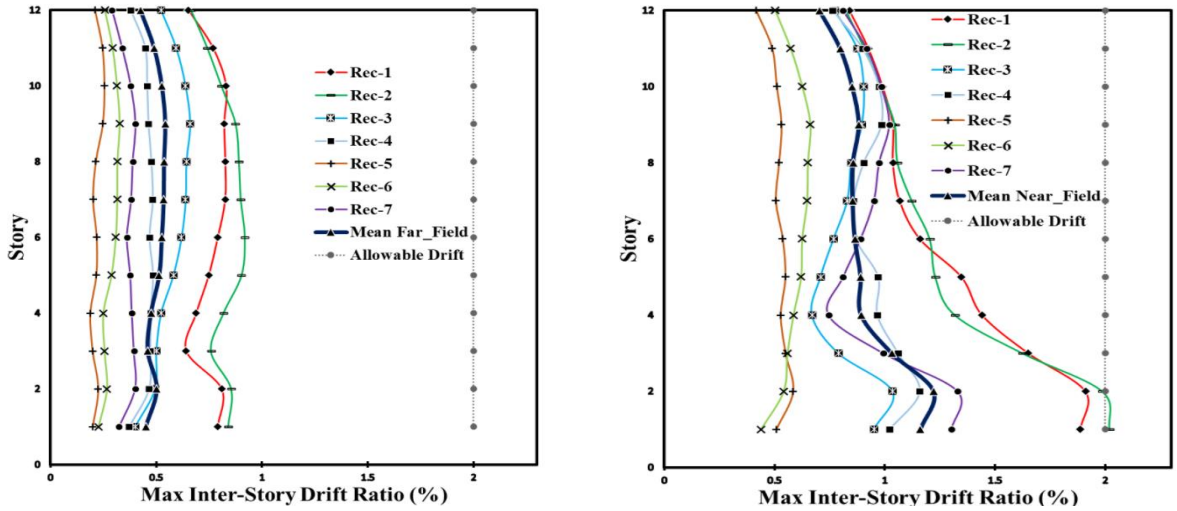

(a) (b)

Fig. 14. Inter-story drift ratio distribution in the12-story structure under: (a) far-fault ground motions at DBE intensity level and (b) near fault ground motions at DBE intensity level.

In **Fig. 18**, **Fig. 19** and **Fig. 20**, the IDA curves illustrate residual drifts for both 8 and 12-story structures under far-fault and near-fault ground motions, within confidence intervals of 99%, 95%, and 90%. At the 90% confidence level, a significant contrast emerges between far-fault and near-

fault ground motions for both structures. Moving to the 95% level, the distinction remains significant only for the 12-story structure. However, at the 99% confidence level, no significant difference between far-fault and near-fault ground motions is observed for either structure.

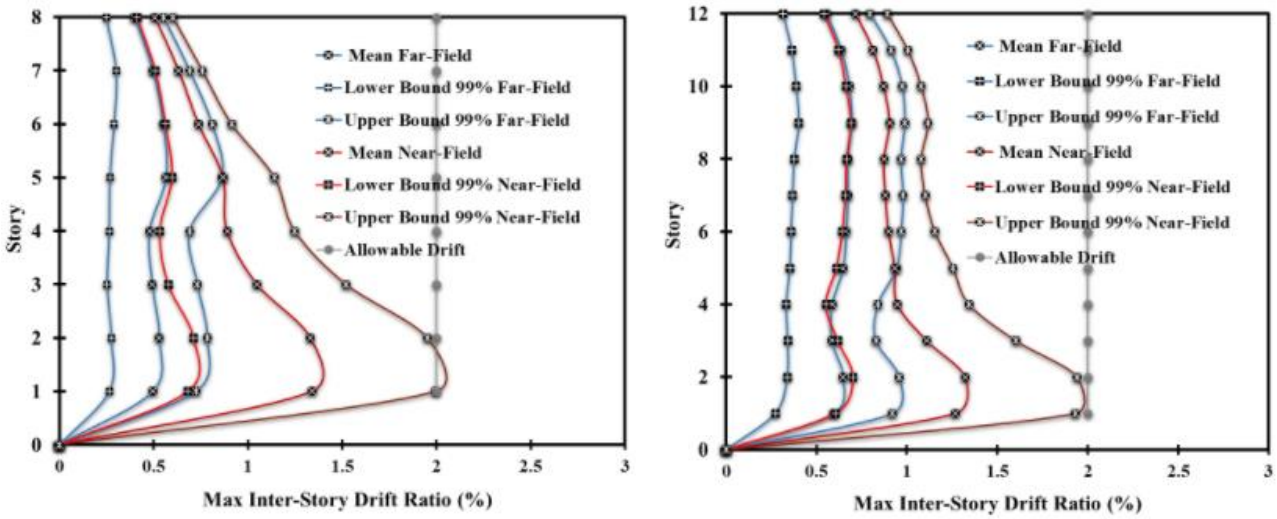

Fig. 15. Comparing 99% confidence intervals for average inter-story drift ratio of far-fault and near-fault ground motions at DBE hazard level: (a) 8-story structure, and (b) 12-story structure.

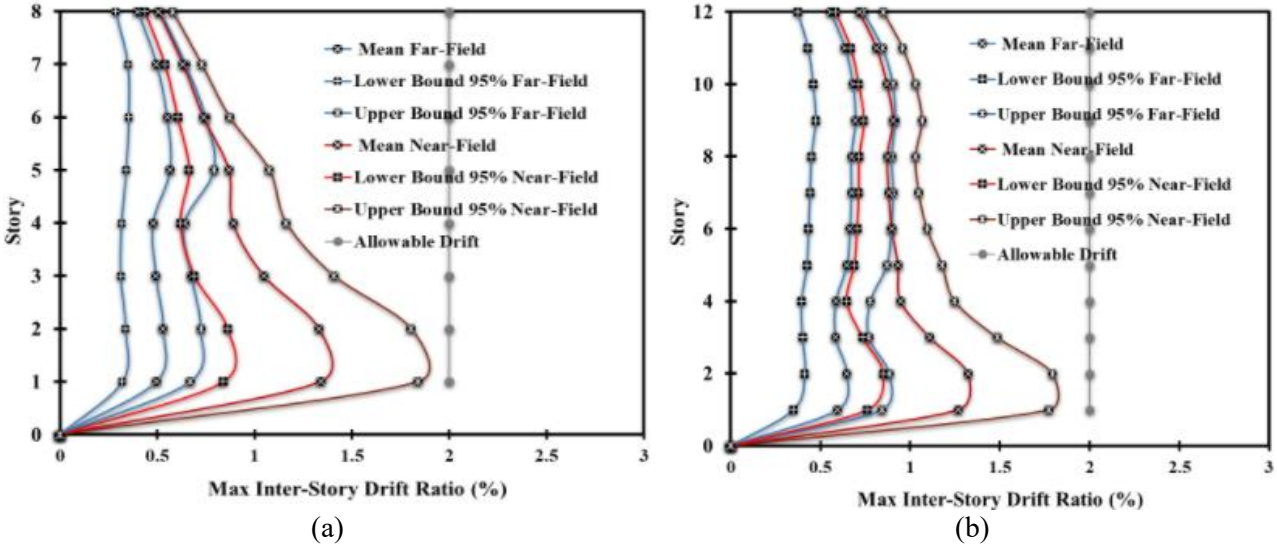

Fig. 16. Comparing 95% confidence intervals for average inter-story drift ratio of far-fault and near-fault ground motions at DBE hazard level: (a) 8-story structure, and (b) 12-story structure.

Fig. 21, **Fig. 22**, and **Fig. 23** illustrate the confidence intervals for residual drifts in 8 and 12-story structures over a hazard return period of 475 years, considering various floors and subjected to far-fault and near-fault ground motions. The distribution of residual drifts varies notably between far-fault and near-fault ground motions. In the case of the 12-story structure, a significant difference between far-fault and near-fault ground motions is evident across all confidence intervals (99%, 95%, and 90%), particularly pronounced in lower floors.

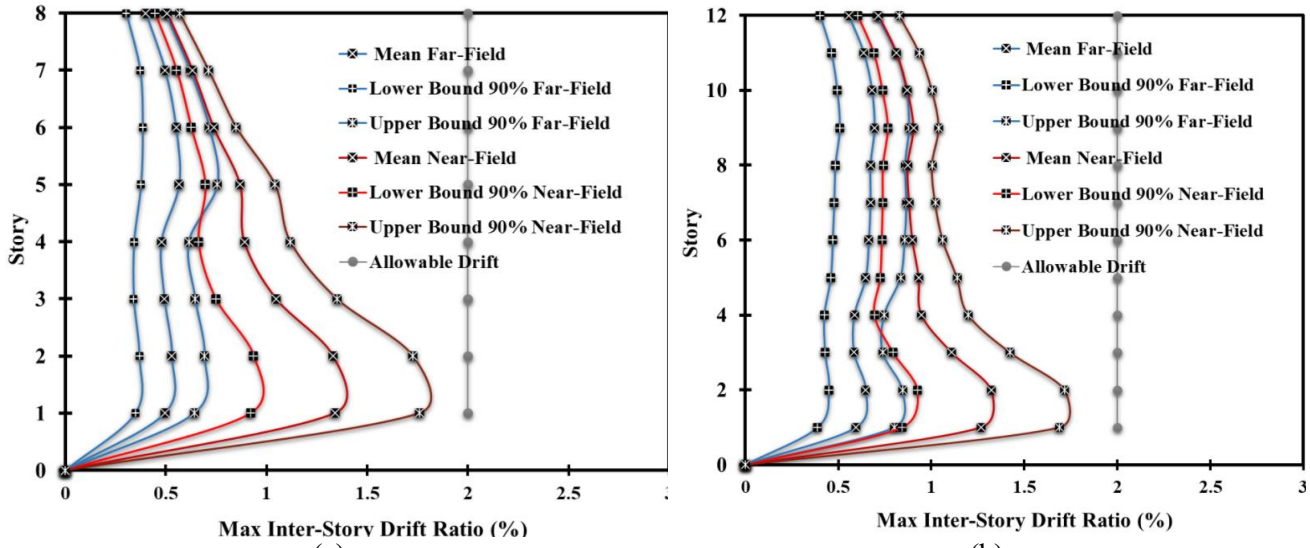

Fig. 17. Comparing 90% confidence intervals for average inter-story drift ratio of far-fault and near-fault ground motions at DBE hazard level: (a) 8-story structure, and (b) 12-story structure.

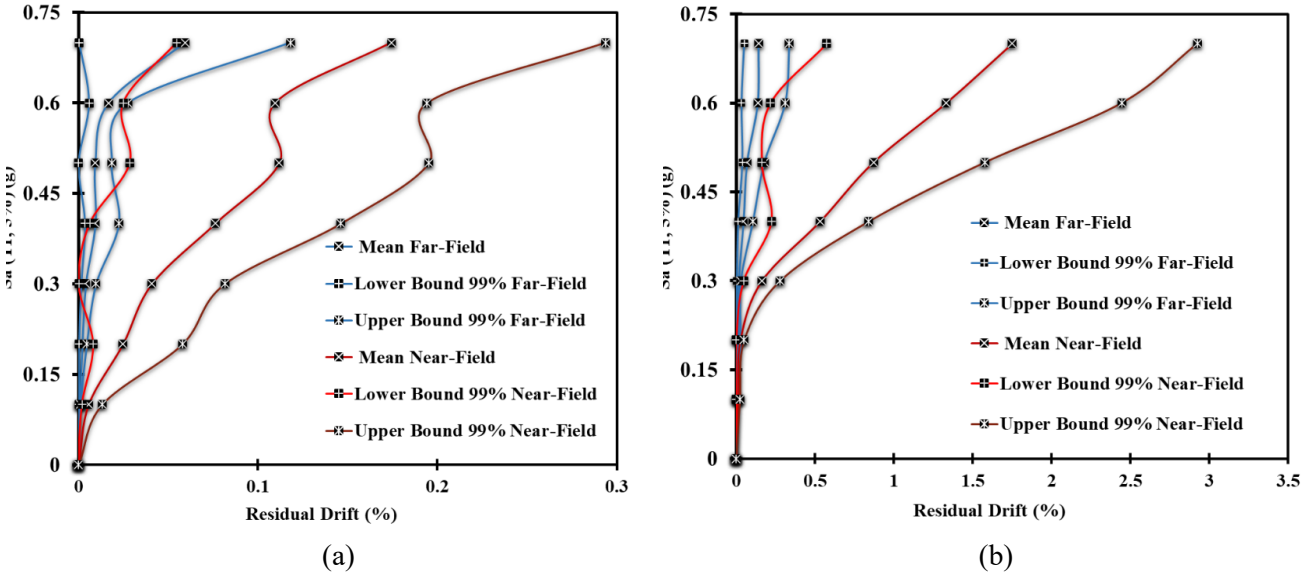

Fig. 18. Comparing 99% confidence intervals for average IDA curves of far-fault and near-fault ground motions in residual drift: (a) 8-story structure, and (b) 12-story structure.

For the 8-story structure, the disparity is less pronounced. In the 99% confidence interval, no significant difference is observed. However, in the 95% confidence interval, a notable difference emerges primarily in the first and second floors, while other floors exhibit no significant distinction. Moving to the 90% confidence interval, a significant difference is observed across all floors, with a more pronounced effect noted in lower floors.

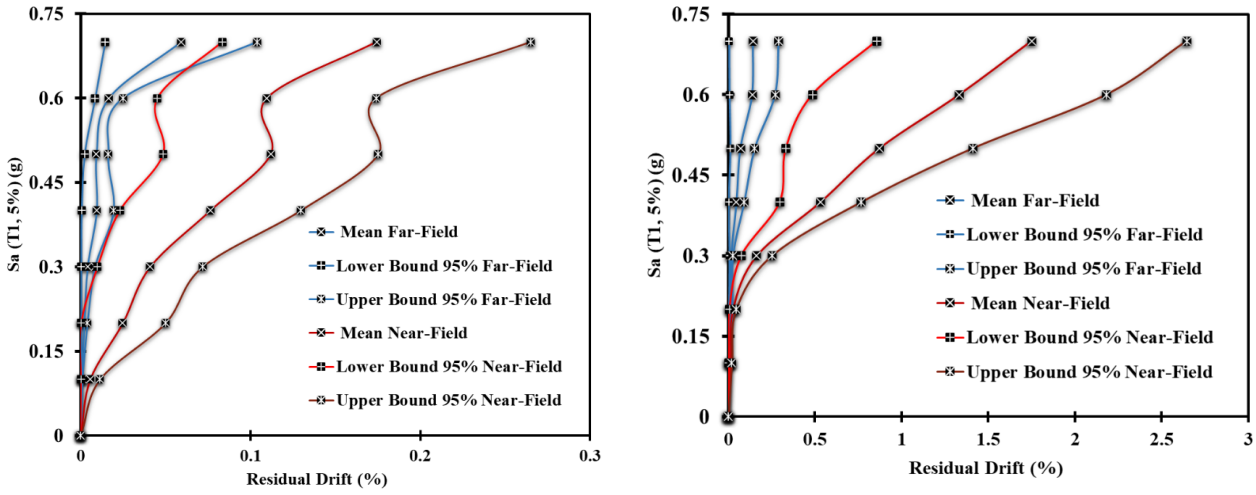

Fig. 19. Comparing 95% confidence intervals for average IDA curves of far-fault and near-fault ground motions in residual drift: (a) 8-story structure, and (b) 12-story structure.

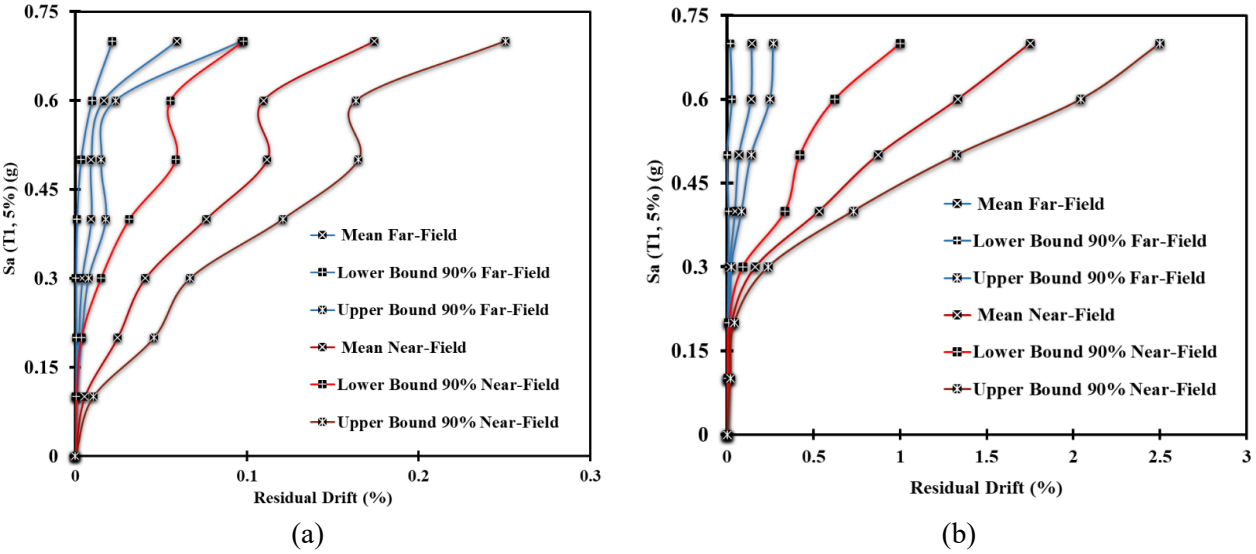

Fig. 20. Comparing 90% confidence intervals for average IDA curves of far-fault and near-fault ground motions in residual drift: (a) 8-story structure, and (b) 12-story structure.

5. Discussion

This study focuses on comparing the effects of near-fault ground motions on the response of BRBF structures from two unique perspectives. First, instead of relying on the average structural response across various records, confidence intervals were employed to provide a more robust comparison. Second, the comparison was conducted at different intensity levels using Incremental Dynamic Analysis (IDA). Additionally, both drift response and residual drift were analyzed for performance assessment. The confidence interval for the average IDA curve, corresponding to the 99% confidence level, shows no substantial distinction between far-fault and near-fault ground motions.

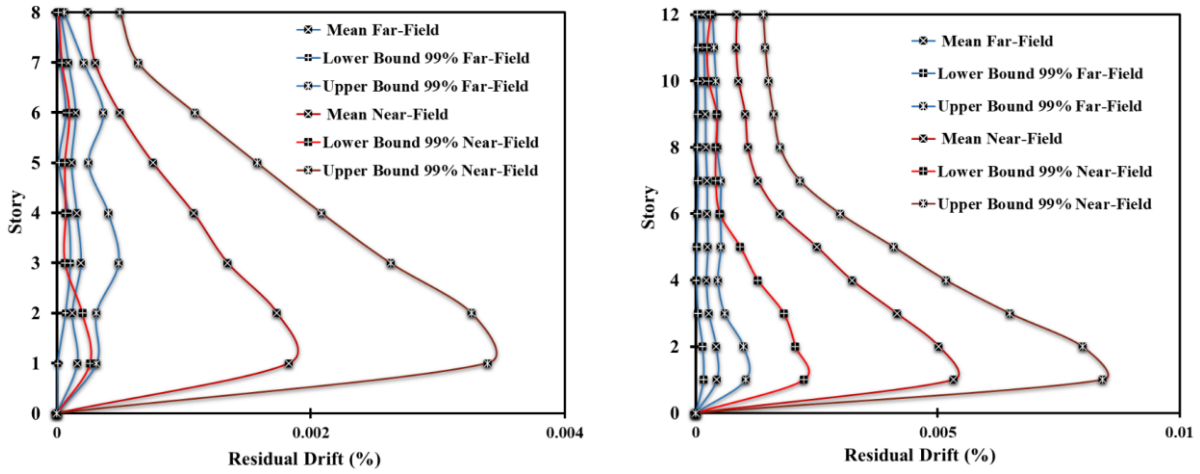

(a) (b)

Fig. 21. Comparing 99% confidence intervals for average residual inter-story drift ratio of far-fault and near-fault ground motions in residual drift at DBE hazard level: (a) 8-story structure, and (b) 12-story structure.

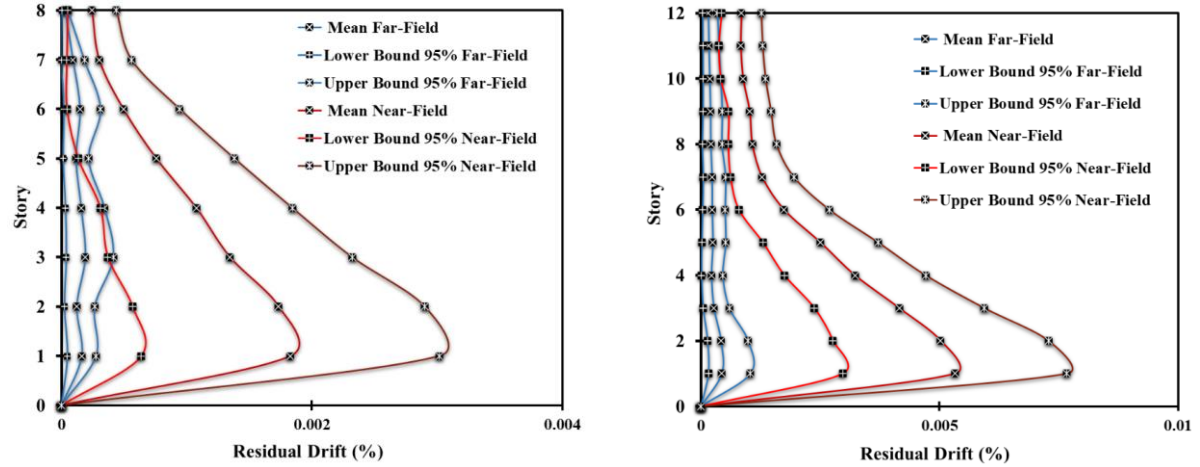

(a) (b)

Fig. 22. Comparing 95% confidence intervals for average residual inter-story drift ratio of far-fault and near-fault ground motions in residual drift at DBE hazard level: (a) 8-story structure, and (b) 12-story structure.

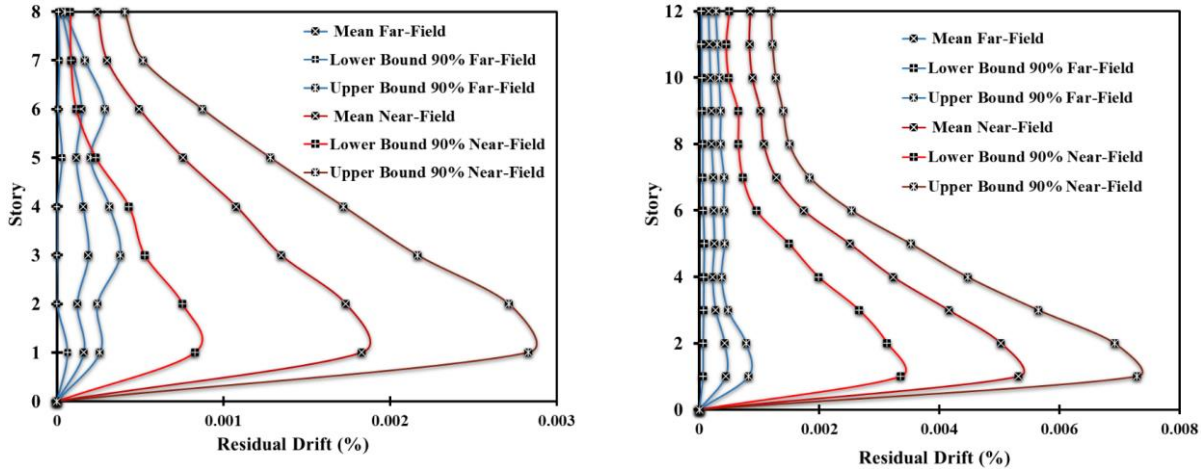

(a) (b)

Fig. 23. Comparing 90% confidence intervals for average residual inter-story drift ratio of far-fault and near-fault ground motions in residual drift at DBE hazard level: (a) 8-story structure, and (b) 12-story structure.

In the context of the 95% confidence level, despite the non-overlapping confidence intervals for the two record sets and an observed difference, this variance is not considered significant. However, at the 90% confidence level, a notable difference of approximately 25% for the 8-story structure and 75% for the 12-story structure becomes evident. Both the 8 and 12-story structures, designed in accordance with seismic regulations, successfully satisfy the inter-story drift ratio criteria.

Notably, the upper limit of the 99% confidence interval in both structures closely approaches the threshold value for the inter-story drift ratio. Among the various confidence levels investigated, the 99% confidence level stands out as the most stringent means of enforcing regulatory compliance. An analysis of the disparity within the confidence interval distributions of average inter-story drift ratios across floors in both 8 and 12-story structures, across three confidence levels (99%, 95%, and 90%), unveils distinct trends between far-fault and near-fault ground motions. At the 99% confidence level, no substantial divergence exists between these two record categories. Shifting to the 95% confidence level, slight and negligible differentiation is observed in the 1st to 4th floors of 8-story structure, while the variation is not pronounced in the upper levels. Turning to the 90% confidence level, the upper floors exhibit no significant differentiation between the record categories, yet a considerable discrepancy comes to the fore in the lower floors. The distribution of inter-story drift ratios across the floors in the examined structures displays notable disparities between responses to far-fault and near-fault ground motions. Specifically, under near-fault ground motions, the inter-story drift ratio distribution on the first and second floors significantly exceeds that of other levels. In contrast, for structures subjected to far-fault ground motions, the distribution tends to be more uniform across all floors. When comparing residual drift between near-fault and far-fault ground motions, the 8- and 12-story structures show no significant difference at the 99% confidence level. At the 95% confidence level, the 8-story structure exhibits no significant difference, while a slight but significant difference appears in the 12-story structure. Notably, at the 90% confidence level, significant differences occur in both the 8- and 12-story structures.

A key limitation of this study is the limited number of structures analyzed. Future work could expand on this by examining the impact of near-fault ground motions on the seismic risk and resilience index of BRBF structures.

Conclusion

The main objective of this study is to compare the seismic behavior of structures with BRBFs under near-fault and far-fault ground motions. Near-fault ground motions are characterized by short, intense pulses. To achieve this goal, the investigation examines two distinct structures: one with eight floors and another with twelve floors, both utilizing BRBFs. These two buildings have been designed following Iran's earthquake-resistant building design regulations. The analysis involves selecting two sets of ground motions: seven categorized as far-fault and seven as near-fault. By employing IDA, response curves are generated to illustrate how these structures respond to both types of ground motions. To establish a comprehensive comparative approach, the focus shifts from a simple averaging of results for each set of far-fault and near-fault ground motions. Instead, the study evaluates the confidence intervals associated with these two record sets. These intervals are assessed at different confidence levels: 99%, 95%, and 90%. This methodology inherently considers the uncertainties that stem from the process of selecting records. The IDA curves for structural drift under the two record categories showed varying differences depending on the confidence level. At the 99% confidence level, no significant difference was observed for either structure. At the 95% level, a significant difference was noted for the 12-story structure, while the 8-story structure showed no significant difference. At the 90% confidence level, significant differences were

observed in both structures, with the 8-story structure showing a 25% variation and the 12-story structure showing a 75% variation. The drift distribution across floors varied between the two record categories. For near-fault ground motions, drift was considerably higher in the lower floors. Similar trends were observed for residual drift. Comparing drift to the permissible limit at the design-based hazard level reveals the following: At the 95th and 90th percentiles, drift for both record categories remains below the permissible limit. However, at the 99% level, the drift for structures under far-fault ground motions is well below the permissible limit, whereas for near-fault ground motions, it slightly exceeds the limit.

Funding

This research did not receive any specific grant from funding agencies in the public, commercial, or not-for-profit sectors.

Conflicts of Interest

The authors declare no known competing financial interests or personal relationships that could have influenced the work reported in this paper.

Authors Contribution Statement

Yaghoub Minaei, Mohammadreza Mashayekhi, Mohammad Sarcheshmehpour: Conceptualization, Data curation, Formal analysis, Investigation, Methodology, Project administration, Resources, Software, Supervision, Validation, Visualization, Writing – review & editing.

Mohammadreza Mashayekhi: Roles/Writing – original draft.

References

[1] Kimura K, Takeda Y, Yoshioka K, Furuya N, Takemoto Y. An experimental study on braces encased in steel tube and mortar. Annu. Meet. Archit. Inst. Japan (in Japanese), 1976.

[2] Wakabayashi M, Nakamura T, Katagihara A, Yogoyama H, Morisono T. Experimental study on the elastoplastic behavior of braces enclosed by precast concrete panels under horizontal cyclic loading—Parts 1 & 2. Summ. Tech. Pap. Annu. Meet., vol. 6, Architectural Institute of Japan; 1973, p. 121–8.

[3] Watanabe A, Hitomi Y, Saeki E, Wada A, Fujimoto M. Properties of brace encased in buckling-restraining concrete and steel tube. Proc. ninth world Conf. Earthq. Eng., vol. 4, 1988, p. 719–24.

[4] Ahmad F, Phillips A. Buckling restrained braced frame seismic response for far-field, near-field, and long-duration earthquakes. J Constr Steel Res 2022;199:107625.

[5] Black CJ, Makris N, Aiken ID. Component testing, seismic evaluation and characterization of buckling-restrained braces. J Struct Eng 2004;130:880–94.

[6] Xie Q. State of the art of buckling-restrained braces in Asia. J Constr Steel Res 2005;61:727–48.

[7] Carden LP, Itani AM, Buckle IG. Seismic performance of steel girder bridges with ductile cross frames using buckling-restrained braces. J Struct Eng 2006;132:338–45.

[8] Castaldo P, Tubaldi E, Selvi F, Gioiella L. Seismic performance of an existing RC structure retrofitted with buckling restrained braces. J Build Eng 2021;33:101688.

[9] Black C, Aiken ID, Makris N. Component testing, stability analysis, and characterization of buckling-restrained unbonded braces (TM). Pacific Earthquake Engineering Research Center; 2002.

[10] Merritt S, Uang C-M, Benzoni G. Subassemblage testing of corebrace buckling-restrained braces. La Jolla, Calif Univ California, San Diego 2003.

[11] Usami T, Kasai A, Kato M. Behavior of buckling-restrained brace members. Stessa 2003, Routledge; 2018, p. 211–6.

[12] Mirtaheri M, Gheidi A, Zandi AP, Alanjari P, Samani HR. Experimental optimization studies on steel core lengths in buckling restrained braces. J Constr Steel Res 2011;67:1244–53.

[13] Chen Q, Wang C-L, Meng S, Zeng B. Effect of the unbonding materials on the mechanic behavior of all-steel buckling-restrained braces. Eng Struct 2016;111:478–93.

[14] Aiken ID, Mahin SA, Uriz P. Large-scale testing of buckling-restrained braced frames. Japan Passiv. Control Symp., Tokyo Institute of Technology Yokohama, Japan; 2002.

[15] Fahnestock LA, Ricles JM, Sause R. Experimental evaluation of a large-scale buckling-restrained braced frame. J Struct Eng 2007;133:1205–14.

[16] Tsai KC, Hsiao BC, Lai JW, Chen CH, Lin ML, Weng YT. Pseudo dynamic experimental response of a full scale CFT/BRB composite frame. Proc., Jt. NCREE/JRC Work. Int. Collab. Earthq. Disaster Mitig. Res., 2003.

[17] Lin ML. Bi-directional sub-structural pseudo-dynamic tests of a full-scale 2-story BRBF, Part 2: Compressive behavior of gusste plates. Proc. 8th US Natl. Conf. Earthq. Eng. 2006. 4, 2006.

[18] Roeder CW. Seismic performance of special concentrically braced frames with buckling restrained braces. 8th Natl. Conf. Earthq. Eng. (8th NCEE), 2006. 4, 2006.

[19] Sabelli R, Mahin S, Chang C. Seismic demands on steel braced frame buildings with buckling-restrained braces. Eng Struct 2003;25:655–66.

[20] Tremblay R, Poncet L, Bolduc P, Neville R, DeVall R. Testing and design of buckling restrained braces for Canadian application. Proc. 13th world Conf. Earthq. Eng., 2004, p. 1–16.

[21] Kiggins S, Uang C-M. Reducing residual drift of buckling-restrained braced frames as a dual system. Eng Struct 2006;28:1525–32.

[22] Fahnestock LA, Sause R, Ricles JM. Seismic response and performance of buckling-restrained braced frames. J Struct Eng 2007;133:1195–204.

[23] Naghavi M, Rahnavard R, Thomas RJ, Malekinejad M. Numerical evaluation of the hysteretic behavior of concentrically braced frames and buckling restrained brace frame systems. J Build Eng 2019;22:415–28.

[24] Asgarkhani N, Yakhchalian M, Mohebi B. Evaluation of approximate methods for estimating residual drift demands in BRBFs. Eng Struct 2020;224:110849.

[25] Asgarian B, Shokrgozar HR. BRBF response modification factor. J Constr Steel Res 2009;65:290–8.

[26] Ariyaratana C, Fahnestock LA. Evaluation of buckling-restrained braced frame seismic performance considering reserve strength. Eng Struct 2011;33:77–89.

[27] Lin P, Tsai K, Wang K, Yu Y, Wei C, Wu A, et al. Seismic design and hybrid tests of a full-scale three-story buckling-restrained braced frame using welded end connections and thin profile. Earthq Eng Struct Dyn 2012;41:1001–20.

[28] Alavi B, Krawinkler H. Strengthening of moment-resisting frame structures against near-fault ground motion effects. Earthq Eng Struct Dyn 2004;33:707–22.

[29] Gerami M, Abdollahzadeh D. Vulnerability of steel moment-resisting frames under effects of forward directivity. Struct Des Tall Spec Build 2015;24:97–122.

[30] Yadav KK, Gupta VK. Near-fault fling-step ground motions: Characteristics and simulation. Soil Dyn Earthq Eng 2017;101:90–104.

[31] Baker JW. Quantitative classification of near-fault ground motions using wavelet analysis. Bull Seismol Soc Am 2007;97:1486–501.

[32] Hoseini Vaez SR, Minaei Z. Pulse extraction of pulse-like ground motions based on particle swarm optimization algorithm. Sci Iran 2020;27:134–58.

[33] Minaei Z, Vaez SRH, Dehghani E, Ezzati E. Quantitative modeling of pulse-like ground motions using imperialist competitive optimization algorithm. J Earthq Tsunami 2023;17:2350003.

[34] Hoseini Vaez SR, Sharbatdar MK, Ghodrati Amiri G, Naderpour H, Kheyroddin A. Dominant pulse simulation of near fault ground motions. Earthq Eng Eng Vib 2013;12:267–78.

[35] Vafaei D, Eskandari R. Seismic response of mega buckling-restrained braces subjected to fling-step and forward-directivity near-fault ground motions. Struct Des Tall Spec Build 2015;24:672–86.

[36] Du K, Cheng F, Bai J, Jin S. Seismic performance quantification of buckling-restrained braced RC frame structures under near-fault ground motions. Eng Struct 2020;211:110447. doi:10.1016/j.engstruct.2020.110447.

[37] Fang C, Zhong Q, Wang W, Hu S, Qiu C. Peak and residual responses of steel moment-resisting and braced frames under pulse-like near-fault earthquakes. Eng Struct 2018;177:579–97.

[38] Shakouri A, Ghodrati Amiri G, Kaviani AA. Evaluation of near-field earthquake-induced pounding in building with friction pendulum bearing considering seismic gap of 360 standard. Civ Infrastruct Res 2023;9:125–40.

[39] Majdi A, Mashayekhi M, Sadeghi-Movahhed A. Effect of Near-Fault Earthquake Characteristics on Seismic Response of Mid-Rise Structures with Triple Friction Pendulum Isolator. J Rehabil Civ Eng 2024;12:47–62.

[40] Soltanmohammadi H, Mashayekhi M, Memarpour MM, Kontoni D-PN, Mirtaheri M. Exploring the Effect of Near-Field Ground Motions on the Fragility Curves of Multi-Span Simply Supported Concrete Girder Bridges. Infrastructures 2024;9:19.

[41] Minaei Z, Vaez SRH, Dehghani E. An approach for estimating the response of steel moment resisting frames to pulse-like ground motions. Soil Dyn Earthq Eng 2021;151:106991.

[42] Vamvatsikos D, Cornell CA. Incremental dynamic analysis. Earthq Eng Struct Dyn 2002;31:491–514. doi:10.1002/eqe.141.

[43] BHRC Publication. Iranian Code of Practice for Seismic Resistant Design of Buildings (Standard No. 2800). 2016.

[44] OpenSEES T. Open system for earthquake engineering simulation (OpenSEES): ver. 3.2. 2 [DB]. Berkeley, CA Pacific Earthq Eng Res Cent (PEER), Univ Calif 2020.

[45] Kalkan E, Kunnath SK. Effects of fling step and forward directivity on seismic response of buildings. Earthq Spectra 2006;22:367–90.

[46] Kardoutsou V, Taflampas I, Psycharis IN. A new pulse indicator for the classification of ground motions. Bull Seismol Soc Am 2017;107:1356–64.